Composites Part B 110 (2017) 255–266

Contents lists available at ScienceDirect

Composites Part B

journal homepage: www.elsevier.com/locate/compositesb

Thermal-mechanical behaviors of CFRP-ECC hybrid under elevated temperatures

Chao Wu [a, b], Victor C. Li [b, *]

[a] School of Transportation Science and Engineering, Beihang University, 37 Xueyuan Road, Beijing 100191, China
[b] Department of Civil and Environmental Engineering, University of Michigan, Ann Arbor, MI 48109, USA

ARTICLE INFO

Article history:
Received 13 May 2016
Received in revised form
28 September 2016
Accepted 15 November 2016
Available online 16 November 2016

Keywords:
Carbon fiber
Hybrid
High-temperature properties
Mechanical testing
Engineered cementitious composite (ECC)

ABSTRACT

Carbon fiber reinforced polymer (CFRP) composites have been accepted for the strengthening of concrete structures. Polymer adhesives are generally adopted for bonding CFRP to the concrete substrate. These polymer adhesives have been facing challenges due to elevated temperatures in fire. Although cementitious adhesives were proposed to replace polymer adhesives, they were found brittle and could hardly sustain high temperatures due to spalling. In the current study, engineered cementitious composite (ECC) was used as the adhesive, and a CFRP-ECC hybrid was externally bonded to the concrete structures for strengthening purpose. ECC shows desirable strain hardening and multi cracking properties in tension, and its anti-spalling behavior has also been proved. This paper presents fundamental studies on the material properties of ECC under elevated temperatures up to 500 °C. The compressive and tensile strengths of ECC under room temperature in this paper were 45.7 MPa and 3.5 MPa respectively. The properties started to drop at 300 °C (compression) and 200 °C (tension). The temperature effects on the interface bonding between CFRP and ECC were also investigated through direct pulled-out tests. Mortar specimens were also prepared for the comparison with the ECC specimens. The experimental results showed that ECC could sustain the elevated temperatures without spalling. The strain hardening and multi cracking behaviors of ECC were observed up to 200 °C. It was also noticed that the interface between CFRP-ECC hybrid and the concrete substrate was sensitive to the elevated temperatures and a method to improve this interface bonding was proposed.

1. Introduction

Carbon fiber reinforced polymer (CFRP) composite has attracted extensive research attentions for strengthening of concrete structures [1–5]. International design guidelines have been published for strengthening of concrete structures using externally bonded CFRP systems [6–10]. This is because CFRP has shown desirable advantages including lightweight, low thermal conductivity, and high resistance to corrosion and chemical attack [11–13]. In the literature, most of the studies [14–20] used polymer based materials (like epoxy) as the adhesive for bonding the CFRP to the surface of the concrete structures. Polymer adhesives can be very effective for strengthening when there are no fire related issues. Otherwise, polymer adhesives undergo significant degradation in their mechanical properties (like modulus and strength), when subjected to elevated temperatures in a fire. This is because when the glass transition temperature (T_g) of a polymer is exceeded, the polymer will change from the glassy state to the rubbery state with a significant reduction in mechanical properties [21–23]. Unfortunately, most of the polymer adhesives used for the structural strengthening have a T_g less than 100 °C [22,24], which is much lower than the elevated temperatures in a fire. Studies suggested that the efficiency of the CFRP strengthening of the concrete structures would extensively reduce (e.g. by 65% at 300 °C as in Ref. [25]) under elevated temperatures [26–28]. This glass transition behavior of the polymer adhesives therefore largely hindered the application of CFRP strengthening for concrete structures which may have fire concerns in their service lives.

A solution to the temperature sensitivity of polymer adhesive is to replace it with cementitious adhesive (like cement mortar) to externally bond the CFRP to the concrete structures [29–32] for strengthening purpose. This is because cementitious adhesives have advantages such as the compatibility with concrete structures, and the capability of sustaining higher temperatures than the

* Corresponding author.
E-mail addresses: wuchao@buaa.edu.cn (C. Wu), vcli@umich.edu (V.C. Li).

http://dx.doi.org/10.1016/j.compositesb.2016.11.037
1359-8368/

polymer counterparts. Unfortunately, cementitious adhesives exhibited intrinsic drawbacks [29,31–35]. Since most of the cement based adhesives are brittle, the load cannot be effectively transferred from concrete to FRP composite. Also the failure generally lacks warning.

The flexural behavior of FRP-strengthened RC beams using cement-based adhesives was studied by Hashemi and Al-Mahaidi [31]. Two layers of CFRP fabric were embedded in a mortar layer of 20 mm thick. The mortar was prepared by mixing ordinary Portland cement and micro-cement with a weight ratio of 1:4. Then the CFRP-mortar hybrid was externally bonded to the concrete beam. The beam was tested under four-point bending setup with a span length of 2.3 m and the strengthening layer was 2 m long. As expected, the loading capacity of the strengthened beam increased by 27%. However, large cracks were observed in the strengthening layer and the mortar detached from the beam due to debonding. Similar study on the flexural strengthening of RC beam using FRP reinforced mortar was conducted by Elsanadedy et al. [35]. The strengthening layer included basalt FRP and mortar. Four-point bending tests were conducted and the experimental results showed that the mortar strengthening layer may debond suddenly from the substrate concrete beam. The authors recommended using polymer-modified mortar for better bonding quality, but this remains essentially a brittle adhesive and would also have fire issues. The maximum increase in the load carrying capacity was found to be 39%. Other researchers also investigated the FRP-mortar system for flexural and shear strengthening [29,33,34], and compared with the FRP using the conventional polymer adhesives [30,35]. It was found that the FRP-mortar system was generally less effective than the FRP-epoxy system in strengthening. For example, it was concluded that FRP-mortar system was 45% [36] and 50% [37] less effective than the FRP-epoxy counterparts. Other researchers claimed that the effectiveness of the FRP-mortar system can be improved through proper design of the strengthening configuration and increased number of FRP layers. Tetta et al. [30] found that the FRP-mortar system can be 92% as effective when two layers of FRP were used in U-wrapped configuration. However, the brittleness of the FRP-mortar system and the concerns in fire condition still remain.

Engineered cementitious composite (ECC) is a promising candidate as the adhesive of CFRP for external strengthening applications [6,7]. ECC is a special class of fiber reinforced mortar [38]. It shows strain-hardening behavior in tension with a strain capacity of at least 3% [39,40], which is on the order of several hundred times that of normal mortar. ECC exhibits multiple cracking during strain-hardening with micro-crack width less than 100 μm [39], making it highly durable in a wide variety of environmental exposure conditions [41–43]. More importantly, ECC can effectively resist spalling failure under elevated temperatures up to 800 °C [44]. Explosive spalling is a common catastrophic failure mode of normal mortars in fire. The anti-spalling behavior of ECC is attributed to the melting of the internal reinforcing fibers (normally polyvinyl alcohol or PVA fibers) [44,45]. The interconnected channels created by the melted PVA fibers are helpful in releasing the internal pressure of ECC under elevated temperatures. Therefore, the concept of using ECC as the adhesive comes from the following two advantages. (1) Polymer adhesive will lose strength at temperatures higher than its glass transition temperature (generally lower than 100 °C) and the CFRP will detach from the structure surface immediately. This is a very dangerous situation because of the lack of the evacuation time. ECC will not fall off and provide longer evacuation time comparing to polymer adhesive. (2) Comparing to mortar adhesive, ECC will not spall under elevated temperatures due to the melting of the internal PVA fibers.

ECC has shown great potential as a repair or strengthening material for bridge decks, and external strengthening layer of concrete beams [46–50]. In a recent study [51], basalt fiber reinforced polymer (BFRP) grid-ECC composite layer was externally bonded to a concrete beam for strengthening purpose in bending. The concrete beam had a span length of 1.7 m with a strengthening layer of 30 mm thick. Six beams were tested in four-point bending with variables including BFRP thickness (1, 3 and 5 mm) and BFRP length (400, 450 and 500 mm). Uniform tiny cracks were observed in the strengthening layer which maintains the integrity during the loading process. The maximum increase in load carrying capacity of the concrete beam was measured as 35%. A similar study on the CFRP-ECC flexural strengthening of concrete beam was reported in Ref. [52]. The ECC was compared with steel fiber reinforced concrete and normal mortar. The strengthened beams were loaded in four-point bending with a span length of 0.86 m. It was found that the use of ECC contributed a good crack dispersing property and deformability to the overlay, and no debonding was observed.

The existing studies on the FRP-ECC hybrid for strengthening of concrete structures focused on the understanding of the failure mechanism and the improvement in the load-carrying capacity. These studies were conducted under room temperature and the anti-spalling advantage of ECC has been neglected. Therefore, fundamental knowledge on the effect of elevated temperatures on the material properties of ECC, particularly the bonding behavior of CFRP-ECC hybrid is lacking.

This paper proposed a CFRP-ECC hybrid as the external bonding layer for strengthening of concrete structures when a structural fire was a concern. The experimental program consisted of two test series. Firstly the compression and tension tests were conducted on ECC which were exposed to elevated temperatures up to 500 °C. The effects of temperature on the compressive and tensile properties of ECC were reported. In the second test series, direct pulled-out tests were conducted to investigate the interface bonding behavior between CFRP and ECC under elevated temperatures up to 500 °C. The failure mode and the stress-slip responses of the pulled-out tests were presented. For comparison purpose, the corresponding mortar specimens were also prepared and tested under the same condition as ECC specimens in both test series. The experimental results in this paper provide fundamental insights on the performance of the CFRP-ECC hybrid for strengthening of concrete structures when subjected to elevated temperatures in a fire.

2. Experimental program

There were two test series in the experimental program, including material testing and pull-out testing. Both tests were conducted under elevated temperatures up to 500 °C. In the material testing, the compression and tension tests were conducted to characterize the temperature effects on the material properties of ECC. In the pull-out testing, the interface behavior between CFRP and ECC under elevated temperatures was investigated. The two test series will be described in the following sections.

2.1. Material testing of ECC under elevated temperatures

The mixture proportion of ECC in the current study is presented in Table 1. The major matrix ingredients of ECC include Type I ordinary Portland cement, Class F fly ash, fine aggregate (F-75 silica sand), water and water reducer (ADVA-190). The fly ash was provided by the DTE Monroe Power Plant in the State of Michigan. The chemical properties of the fly ash provided by the manufacturer are listed in Table 2. The F-75 silica sand has a maximum and an average grain size of 250 μm and 110 μm, respectively. The Poly-Vinyl Alcohol (PVA) fibers are 12 mm long with a diameter of

Table 1
Mixture proportion of ECC in the current study (kg/m^3).

Water (W)	Cement (C)	Fly ash (FA)	Silica sand	PVA fiber	Water reducer	W/(C + FA)	FA/C
311	393	865	457	26	5	0.25	2.20

Table 2
Chemical composition and physical properties of fly ash provided by manufacturer.

Chemical composition, %	Fly ash
CaO	15.66
SiO_2	42.20
Al_2O_3	22.51
Fe_2O_3	9.20
SO_3	1.85
MgO	3.20
Na_2O	0.98
K_2O	1.53
Moisture	0.12
Loss on ignition	1.34
Physical properties	
Fineness, % retained on#325	16.58
Water requirement, %	95
Specific gravity	2.53

39 μm. The PVA fibers are coated with 1.2% by weight of oil to control the fiber/matrix interfacial properties. The volume content of PVA fiber in ECC was 2%. The detailed information of the PVA fiber has been well documented in the publications by the ACE-MRL group at the University of Michigan [44,45,53] and is summarized in Table 3.

The ECC mixture was prepared in a Hobart type mixer of 10 L capacity. Firstly, cement, sand and fly ash were dry mixed for 5 min at a speed of 98 r/min. Then the mixture of water and water reducer was added and mixed for another 4 min under the same speed. Then the mixture was checked and any clumpings were broken to ensure a homogeneous paste status. The mixing continued for another 2 min until the paste reached a good fluidity. Then the PVA fibers were added slowly into the mortar and mixed for 5 min at a speed of 198 r/min. The mixture was checked again for fiber agglomeration. Finally, the mixing continued for another 3 min until the fibers were well dispersed.

The fresh ECC was cast into the molds that were moderately vibrated using a vibration table. It was noted that, the followability of fresh ECC was reasonable and could wet the concrete surface though its fluidity reduced a little due to the addition of PVA fibers. This fluidity was also checked by other researchers for strengthening purpose [51,52,55]. The molds were sealed with plastic bags and subsequently demolded after 1 day curing. All specimens were cured for another 27 days in air (23 ± 3 °C; 30± 10% RH). Both cube specimens and dogbone-shaped specimens were prepared for the subsequent compression and tension testing respectively. The cube specimens had a dimension of 50 × 50 × 50 mm^3 according to ASTM C190/C190 M [54]. The dimensions of the dogbone-shaped specimens can be found in Ref. [55], which were recommended by the Japan Society of Civil Engineers (JSCE) [56] for standardized tensile testing of ECC.

Table 3
Properties of PVA fiber [42,43,50].

Diameter (μm)	Length (mm)	Nominal strength (MPa)	Modulus (GPa)	Density (kg/m^3)	Melting point (°C)
39	12	1600	42	1300	230

After 28 days curing time, both cube and dogbone-shaped specimens were heated in a Vulcan 3–550 muffle furnace from DENTSPLY International Inc. The target temperature was selected at every 100 °C up to 500 °C at a heating rate of 5 °C/min. When the target temperature was reached, it was held for one hour to make sure the temperature of the specimen became uniform and stable [44]. Then the specimens were taken out of the furnace and cooled down to the room temperature, after which the compression and tension tests were conducted. Specimens without temperature treatment were also prepared for comparison purpose.

The compression tests were conducted on a FORNEY F–50 F–F96 machine under a load control at a speed of 20 MPa/min. The peak load was recorded to determine the compressive strength. The tension tests were carried out on a servo-hydraulic Instron 5969 testing system with a capacity of 50 kN. A displacement control was adopted with a speed of 0.5 mm/min. The experimental setup of the tensile testing is presented in Fig. 1. Two linear variable displacement transducers (LVDT), with a gage length of approximately 100 mm, were attached to the specimen. Stress-strain curves were then recorded to determine the behavior of specimens under direct tension.

For comparison purpose, mortar cube and dogbone specimens (ECC without PVA fibers) were also prepared. The preparation process and testing setup were all the same as ECC specimens. Mortar dogbone specimens were not exposed to elevated temperatures and only room temperature specimens were tested. Mortar cube specimens were treated with the same target temperatures as ECC cubes for comparison purpose.

2.2. Pull-out testing of CFRP-ECC hybrid under elevated temperatures

Direct pull-out tests were conducted in order to investigate the interface behavior between CFRP and ECC of the hybrid system. Since this system was proposed for strengthening of concrete structures, a concrete block was also included when preparing the pull-out specimen. The dimensions of the specimen and the experimental setup are presented in Fig. 2. The specimen was

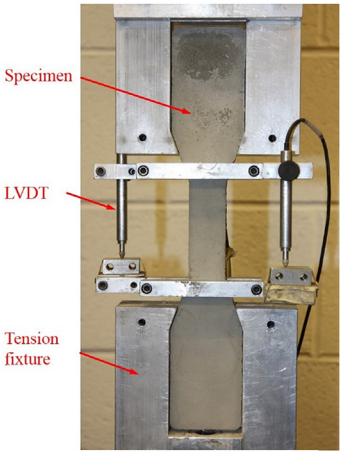

Fig. 1. Experimental setup of tensile tests.

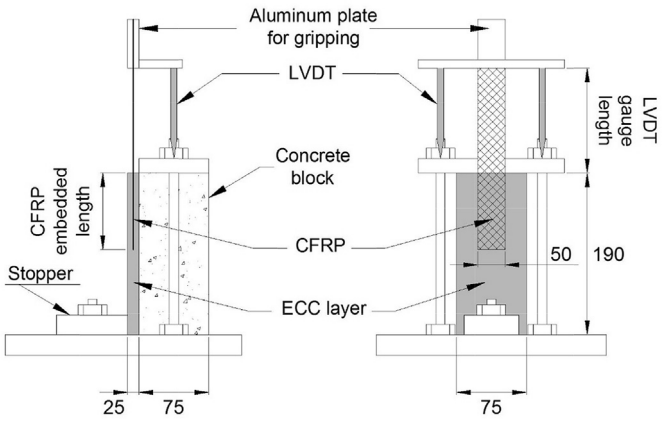

Fig. 2. Experimental setup of pull-out tests and specimen dimensions (unit in mm, not to scale).

seated on a steel base plate and was secured in position by the top steel plate which was fastened to the base plate through two steel rods. A stopper was mounted on the base plate to prevent any lateral movement of the specimen during the loading process. The stopper can be adjusted when installing the specimen so that the CFRP sheet was in the vertical direction. A spirit level was used to check the straightness of the CFRP sheet before testing. The CFRP sheet was 50 mm wide and was embedded in the middle of the ECC layer which was attached to the concrete block. Two LVDT were used to record the relative movement of the CFRP sheet and the ECC. The LVDT were the same as those in Fig. 1. The gauge length of each specimen was recorded and used for calculation of the relative slip between CFRP and ECC (see the detailed discussions in Section 3.2).

CFRP sheet was Tyfo SCH-41 provided by MTC Corporation in St. Louis with a measured thickness of 0.55 mm. The tensile tests were conducted according to the ASTM D3039 [57]. The tensile strength was not achieved due to the difficulty of clamping CFRP sheets. The tested modulus was 79.7 GPa on average with the applied stress up to 833.5 MPa. Six repeating tests were conducted to measure this modulus. The nominal tensile strength of the CFRP sheet was 986 MPa. The mixture proportion of ECC was the same as that in Table 1. The concrete mixture is presented in Table 4. The compression strength of the concrete was tested using concrete cylinder of 75 mm diameter according to ASTM C873/C873 M [58]. The 28-day compressive strength was 40.5 MPa.

The preparation procedure of the pull-out specimens is presented in Fig. 3. Firstly, the surface of the concrete block was prepared after 28 days of curing. The cement on the surface was removed and the course aggregates were exposed. The purpose of the surface treatment was to ensure the bonding quality between the hybrid layer and concrete, so that this interface would not be a problem during the pull-out tests. Then the concrete blocks were placed in a mold, where the CFRP sheets can be secured in position. The first layer of the fresh ECC of 12.5 mm thick was applied on top of the concrete block and underneath the CFRP sheet. Finally another layer of ECC of 12.5 mm thick was casted on top of the CFRP sheet. The thickness of the ECC layer was 25 mm with a CFRP embedded length of 100 mm. 100 mm embedded length was selected for analyzing the temperature effects on the bond behavior between CFRP and ECC. 100 mm was lower than the effective bond length of CFRP in ECC which was measured in another pull out tests under room temperature. The results of these pull out tests will be reported elsewhere. The specimens were demolded after 1 day and cured for another 27 days in air (23 ± 3 °C; 30± 10% RH). Because the concrete block was cured for 56 days before pull-out tests, its 56-day compressive strength was also tested which was 41.7 MPa (only 3% higher than its 28-day strength which was 40.5 MPa).

Table 4
Mixture proportion of concrete (kg/m^3).

Water	Cement	Stone	Sand
200	476	1105	562

After 28 days curing of the ECC layer, the pull-out specimens were heated in the muffle furnace under various target temperatures up to 500 °C. The specimens were left in the furnace for one hour after the target temperature was reached. Then the specimens were taken out and cooled down to the room temperature. The pull-out tests were conducted on a MTS 810 material testing system with a loading capacity of 100 kN. The displacement control was used with a loading speed of 0.5 mm/min. The pull-out test was continued until the load dropped dramatically or the CFRP sheet was pull out by 30 mm from LVDT reading.

For comparison purpose, pull-out specimens were also prepared with CFRP embedded in a mortar layer (CFRP-mortar hybrid comparing with CFRP-ECC hybrid). The mixture proportion of the mortar was the same as that of ECC but without PVA fibers. The specimen preparation process, loading scheme and temperature treatment were kept the same as the specimens with CFRP-ECC hybrid.

3. Experimental results and discussions

3.1. Effect of elevated temperatures on the material properties of ECC

In the material testing, six target temperatures were selected including room temperature (23 °C), and elevated temperatures up to 500 °C at every 100 °C. The cube specimens after temperature treatment are compared in Fig. 4. It can be seen in Fig. 4(a) that the PVA fibers could be observed on the surface of the ECC cubes when the temperature was lower than 200 °C. When the temperature was higher than 300 °C, no PVA fibers were remained on the cube surface. This is because the PVA fibers had melted at such high temperatures with a melting point of 230 °C (see Table 3).

In order to visually prove the melting process, a bunch of PVA fibers were heated in the muffle furnace up to 600 °C and the color and phase change of the fibers are shown in Fig. 5. It can be seen that the fibers became light brown at 200 °C and changed to dark brown at 250 °C. Then the bundle was carbonized and became black from 300 °C to 400 °C. At 500 °C the fibers started burning and fully decomposed at 600 °C.

In order to quantify this decomposition process of PVA fibers, thermogravimetric analysis (TGA) was conducted in air using a TGA Q5000 IR from TA Instruments. 3–5 mg fibers were placed in an aluminum pan. The temperature was raised from room temperature to 700 °C with a heating rate of 5 °C/min. The TGA test was also performed on the carbon fibers which were cut from the CFRP sheet. The TGA results of the PVA fiber and the carbon fiber are compared in Fig. 6. It can be seen that the carbon fiber was more thermal stable and only started decomposition at about 600 °C. The PVA fiber started decomposition at about 200–250 °C. The decomposition process of PVA fiber completed at around 550 °C.

Another interesting observation in Fig. 4 is that surface cracks were observed on mortar cubes when the temperature exceeded 300 °C. The mortar cube spalled under 400 °C and 500 °C. The spalling is a catastrophic failure of cementitious material which generally occurs during a fire. It is believed that spalling is related to the increased internal pressure created by the water vapor under

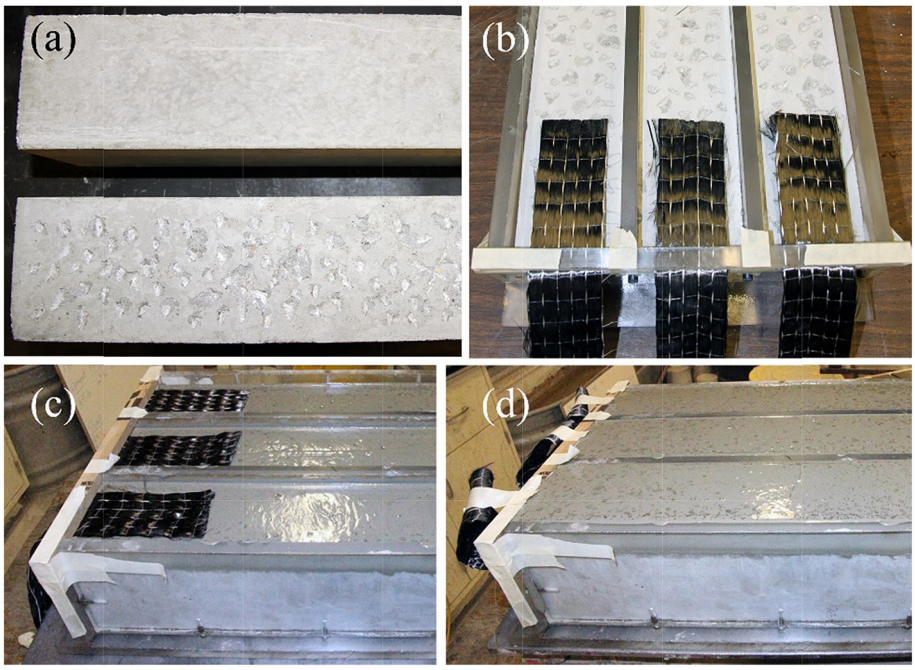

Fig. 3. Preparation process of pull-out specimens: (a) surface treatment of concrete block; (b) CFRP sheet positioning; (c) apply the first layer of ECC and (d) apply the second layer of ECC.

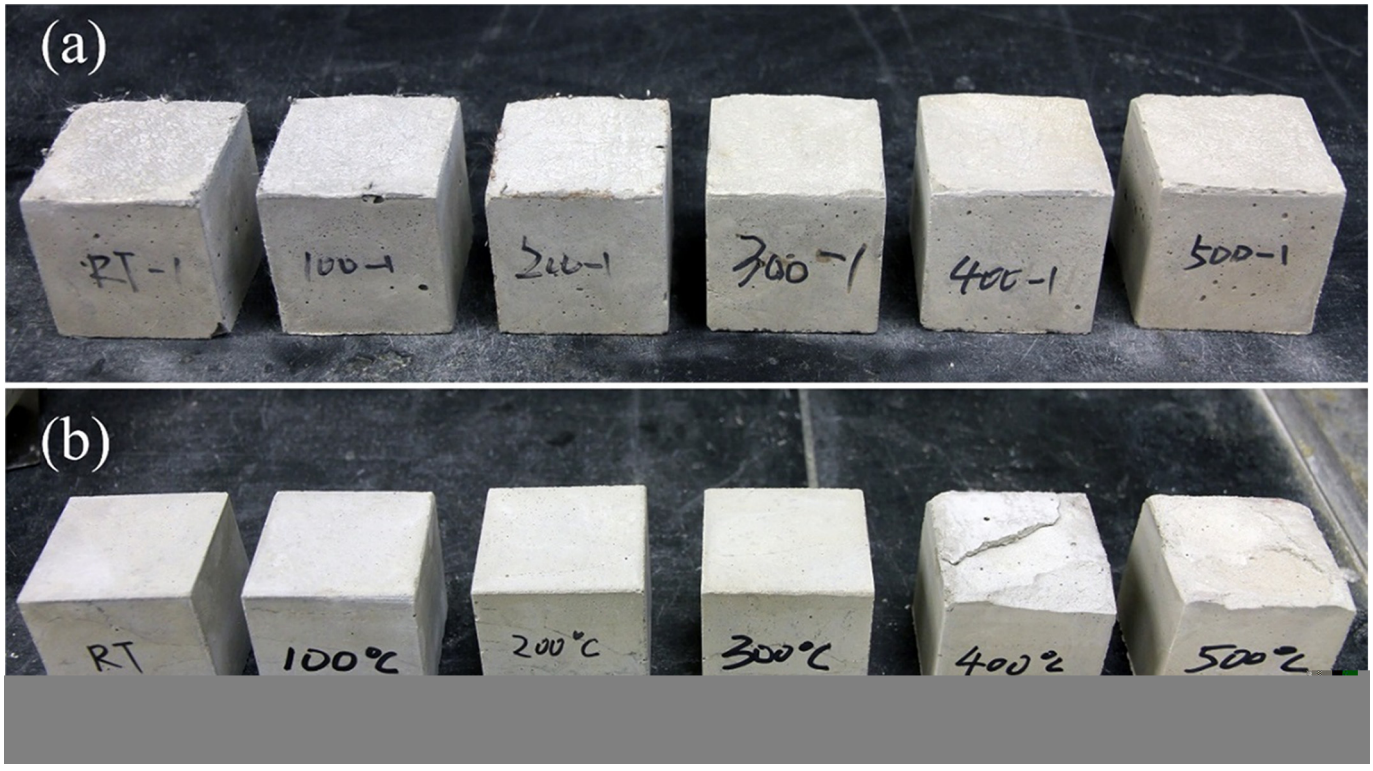

Fig. 4. Comparison after temperature treatment: (a) ECC cubes and (b) mortar cubes.

elevated temperatures [59,60]. On the other hand, no cracks or spalling were observed on the ECC cubes up to 500 °C. This is because the PVA fibers melted under high temperature leaving a network of interconnected channels. Water vapor in ECC can then escape through these interconnected channels without creating detrimental internal pressure. Scanning electron microscope (SEM) images in Fig. 7 were taken on the ECC before and after the temperature treatment, and the channels left by the melted PVA fibers can be clearly observed. The mechanism of the water vapor escaping through the interconnected channels left by the melted

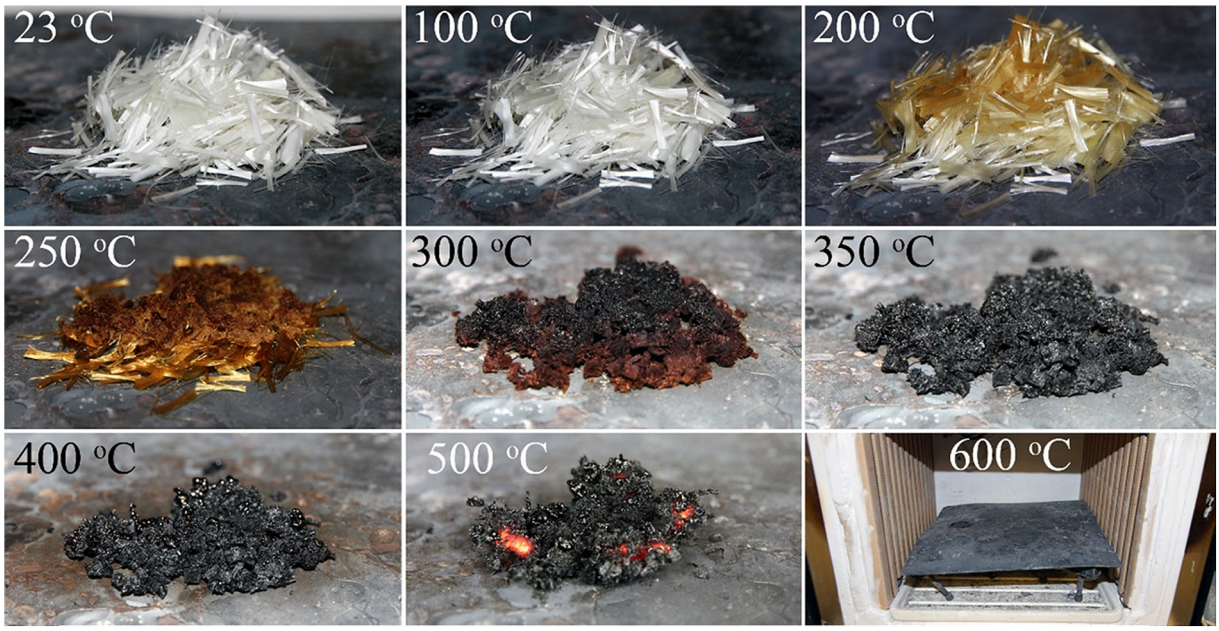

Fig. 5. Color and phase change of PVA fibers under elevated temperatures. (For interpretation of the references to colour in this figure legend, the reader is referred to the web version of this article.)

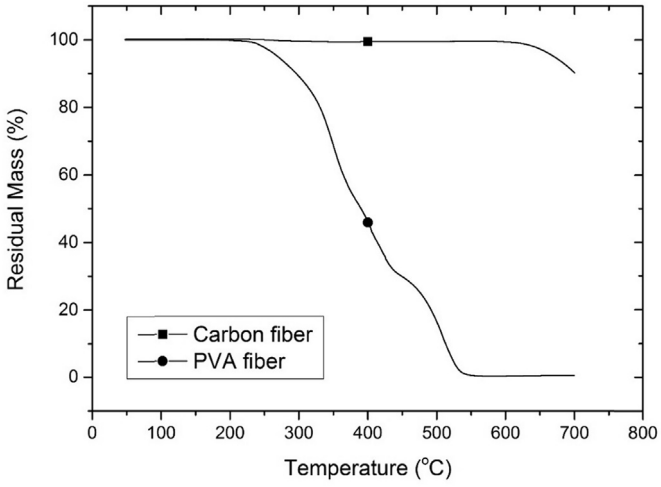

Fig. 6. TGA results of the PVA and carbon fibers.

PVA fibers of ECC has been well discussed by Sahmaran et al. [44].

After the temperature treatment, the cubes were cooled down to room temperature and tested under compressive loading. The compressive strengths of ECC and mortar cubes under various temperatures are plotted in Fig. 8. The results of ECC cubes were denoted using solid square symbols while those of mortar cubes were presented using hollow square symbols. At least six specimens were tested for each temperature and the error bar in Fig. 8 represents the corresponding standard deviation.

For ECC cubes, the compressive strength did not change much at 100 °C (45.4 MPa) comparing to the strength at room temperature (45.7 MPa). The strength at 200 °C was 43.5 MPa, showing a 4.8% decrease, and then became constant up to 300 °C (43.3 MPa). The compressive strength dramatically decreased by 20.8% at 400 °C with a strength of 36.2 MPa. At 500 °C, only 68.7% of the compressive strength at room temperature remained (31.4 MPa). Therefore, the effect of the temperature on the compressive strength of ECC can be divided into two stages with the turning point at 300 °C.

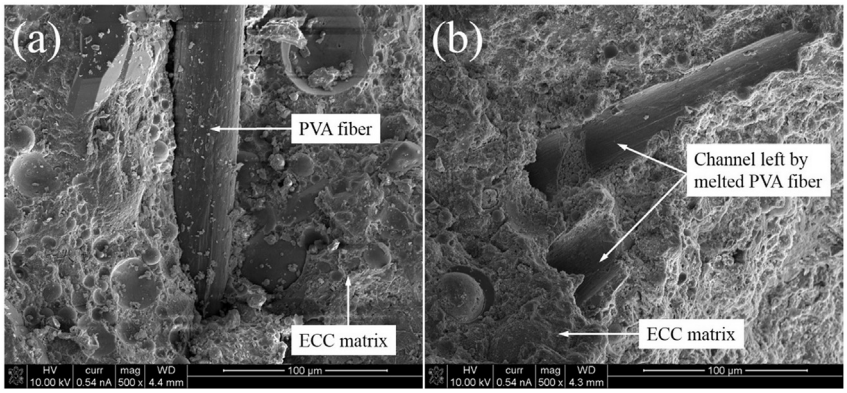

Fig. 7. SEM images of ECC at (a) room temperature and (b) 500 °C.

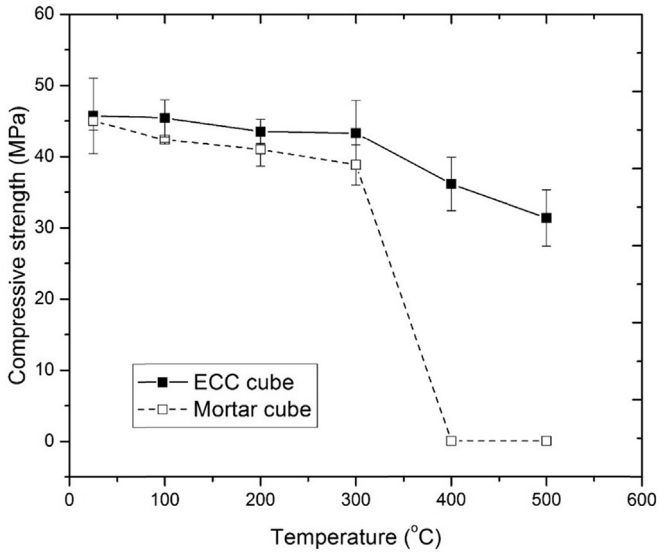

Fig. 8. Temperature effect on the compression strength of the ECC and mortar cubes.

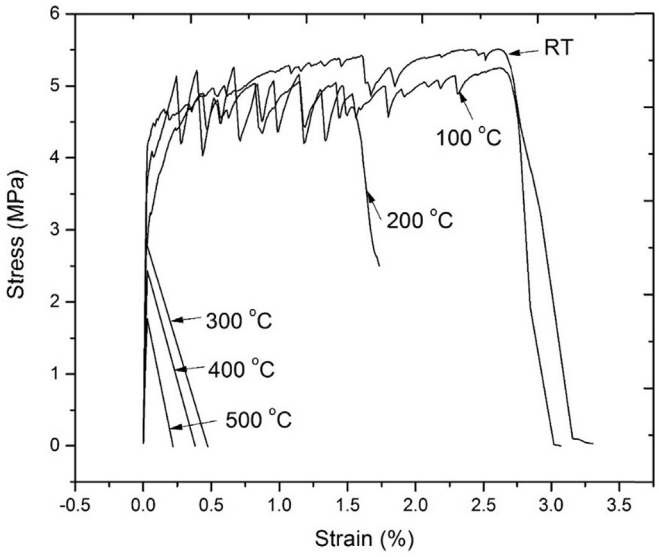

Fig. 9. Temperature effect on the tensile stress-strain curves of ECC dogbone-shaped specimens.

There are two mechanisms contributing to the two-stage strength development of ECC under elevated temperatures. Both mechanisms are related to the melting of PVA fibers. Firstly, the melting of PVA fibers created interconnected channels (Fig. 7), which allowed the water vapor to escape and consequently relieved the internal pressure of ECC [44]. This mechanism is helpful to reduce the internal cracks due to water vapor pressure under elevated temperatures. The second mechanism is that the interconnected channels became the crack initiation sites making the cube more susceptible to fracture under loading [45]. Considering these two mechanisms, the two-stage strength development of ECC under elevated temperatures can be revealed. Under a moderate temperature up to 300 °C, the first mechanism was dominant since very few PVA fibers were melted (see Fig. 6). Therefore, the temperature had little effect on the compressive strength of ECC in the first stage. When the temperature was higher than 300 °C, the PVA fibers started melting quickly as evidenced by the TGA curve in Fig. 6. With more interconnected channels generated, the second mechanism became dominant and the interconnected channels became internal defects. This resulted in a dramatic decrease in the compressive strength of ECC.

Similarly, the two-stage temperature effect on the compressive strength of the mortar cubes was also observed in Fig. 8. In the first stage, the strength decreased slowly from 45.0 MPa at room temperature to 38.8 MPa at 300 °C, showing a 13.8% strength reduction. The compressive strengths at 100 °C and 200 °C were 42.4 MPa and 41.0 MPa, respectively. In the second stage, the strength dropped to zero because the cubes spalled in the furnace, making it impossible to do the compression tests. The mortar cubes had the same mixture as the ECC cubes without PVA fibers. That means the mortar cubes had a dense microstructure due to the significantly low water to cement ratio, high fly ash cement and an absence of course aggregate [44]. This dense material was more susceptible to the internal cracks induced by the water vapor pressure under elevated temperatures. Since the mortar cubes lack the pressure releasing mechanism through the melting of PVA fibers, the compressive strength became more sensitive to the temperature-induced degradation.

The typical tensile stress-strain curves of the ECC dogbone-shaped specimens under various temperatures are presented in Fig. 9. The peak stress and the corresponding strain of the stress-strain curve in Fig. 9 were defined as “tensile strength” and “tensile strain capacity”, respectively [56]. In the case when slight stress decrease after the peak stress was observed, the strain at 95% of the peak stress was used as the “tensile strain capacity” [55]. The tensile strength and tensile strain capacity of ECC dogbone specimens are shown in Fig. 10. At each temperature, the symbol represents the average value and the error bar is the standard deviation of the four repeating specimens. For comparison purpose, six mortar dogbone specimens were prepared and tested only under the room temperature. The average tensile strength was 3.5 MPa with a standard deviation of 0.3 MPa. The average tensile strain capacity was 0.011% with a standard deviation of 0.002%. The tensile strain hardening behavior of ECC under room temperature is obvious in Fig. 9. Little change in the strain capacity was observed at 100 °C. The strain capacity started decreasing at 200 °C and brittle failure occurred at a temperature no less than 300 °C.

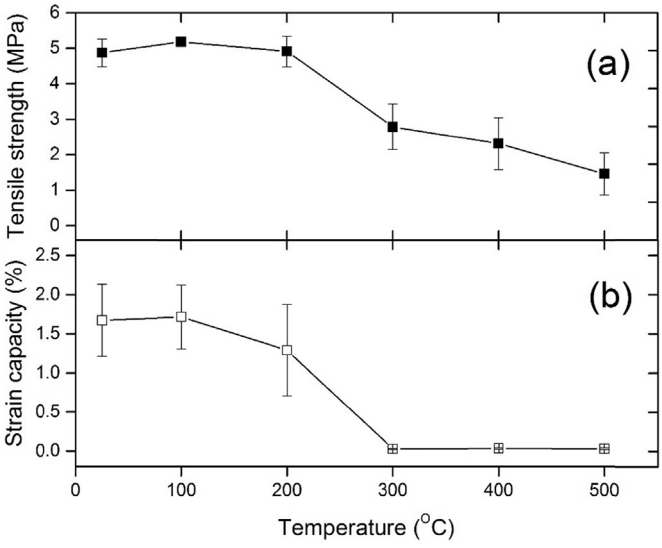

Fig. 10. Temperature effect on the tensile properties of ECC dogbone-shaped specimens: (a) tensile strength and (b) tensile strain capacity.

Similar to the compression results in Fig. 8, a two-stage behavior was observed in Fig. 10 for both tensile strength and tensile strain capacity with the elevated temperatures. However, the turning point changed to 200 °C. At room temperature, the tensile strength of ECC was 4.9 MPa with a strain capacity of 1.7%. Comparing to the mortar, the tensile strength of ECC increased by 40% (from 3.5 to 4.9 MPa) and the strain capacity improved by 153 times (from 0.011% to 1.7%). The tensile strength of ECC showed little change when the temperature reached 200 °C (4.9 MPa), whereas the strain capacity decreased to 1.3%. After 200 °C, the strength and strain started to decrease dramatically. At 300 °C and 400 °C, the tensile strength of ECC reduced to 2.8 MPa and 2.3 MPa respectively. At 500 °C, the strength decreased by 69.4% to 1.5 MPa. The ECC dogbone-shaped specimens exhibited brittle failure when the temperature went above 200 °C, and the strain capacity dropped to 0.03%. The two mechanisms by which the elevated temperatures affected the compressive strength of ECC are still valid for the tension properties.

It is also interesting to observe that the strength and strain capacity increased at 100 °C comparing to the properties under room temperature. For example, the strength at 100 °C was 5.2 MPa with a strain capacity of 1.7%. This increase in tensile strength and strain capacity was also observed by Yu et al. [45]. It was found in Ref. [45] that the fiber strength and the fiber/matrix interface properties improved with the temperature up to 100 °C. These properties dramatically decreased with the temperature higher than 200 °C. This observation indicates that a moderate temperature treatment up to 100 °C can effectively enhance the tensile properties of ECC.

3.2. Effect of elevated temperatures on the interface behavior of CFRP-ECC hybrid

Pull-out tests were conducted to investigate the effect of temperature on the interface behavior between CFRP and ECC. The specimens were left in the muffle furnace under a constant temperature for one hour and cooled down to room temperature before the pull-out tests. For each temperature, at least three specimens were tested for repeating purpose. The detailed specimen preparation and experimental setup can be found in Section 2.2.

The pull-out specimens after the temperature treatment are compared in Fig. 11(a) for ECC specimens and Fig. 11(b) for mortar specimens, respectively. The image of the bottom surface of each specimen was taken which showed clearly the concrete block, hybrid layer and their interface. It is obvious that the surface color of both ECC and mortar specimens gradually became darker due to the temperature treatment. Similar to the ECC cubes in Fig. 4(a), the PVA fibers cannot be observed on ECC specimens when the temperature was higher than 300 °C. It is important to examine the effect of temperature on the interface between the concrete and the hybrid layer in Fig. 11. As for the ECC specimens in Fig. 11(a), the interface was intact at 100 °C. At 200 °C, a tiny crack was observed at the interface. The crack became more obvious at 300 °C and 400 °C. When the temperature increased to 500 °C, all the three repeating specimens failed with the hybrid layer separated from the concrete block. On the other hand, the interface of mortar specimens in Fig. 11(b) showed better temperature resistance. For example, no obvious interface crack was observed up to 300 °C. At 400 °C, the interface crack became clear and at 500 °C, one of the three repeating mortar specimens had the hybrid layer fell off from the concrete block.

As introduced in Section 2.2, the concrete surface was treated to expose the coarse aggregate before bonding the hybrid layer. Comparing with fresh mortar, ECC show much higher viscosity with reduced followability due to the addition of the PVA fibers. Therefore, it became more difficult for ECC to spread and fill the gaps on the concrete surface. Under the heating and cooling conditions during the temperature treatment process, the interface was subjected to the expansion and contraction difference between the hybrid layer and concrete, and therefore, more susceptible to the interface cracking. This is the reason why the interface of ECC specimens showed higher degradation under elevated temperatures.

During the pull-out tests, two different failure modes were observed for ECC specimens. The CFRP sheet were pulled out from the ECC layer when the temperature was not higher than 200 °C. The failure mode changed to the interface separation between the CFRP-ECC hybrid layer and the concrete with higher temperatures than 200 °C (see Fig. 12(a)). This interface separation failure agrees with the observation in Fig. 11(a), which showed that the interface started to degrade at 200 °C before the pull-out test. When the CFRP sheet was loaded, the interface could hardly sustain the shear loading and the hybrid layer finally separated from the concrete.

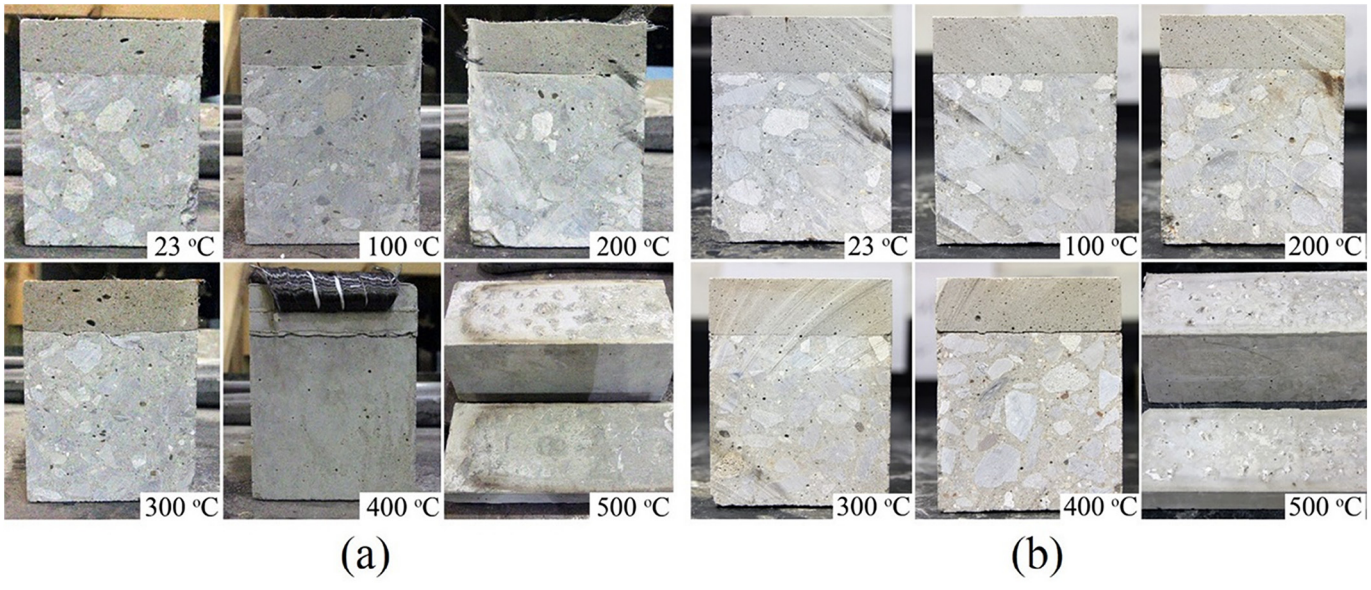

Fig. 11. Pull-out specimens after the temperature treatment: (a) ECC specimens and (b) mortar specimens.

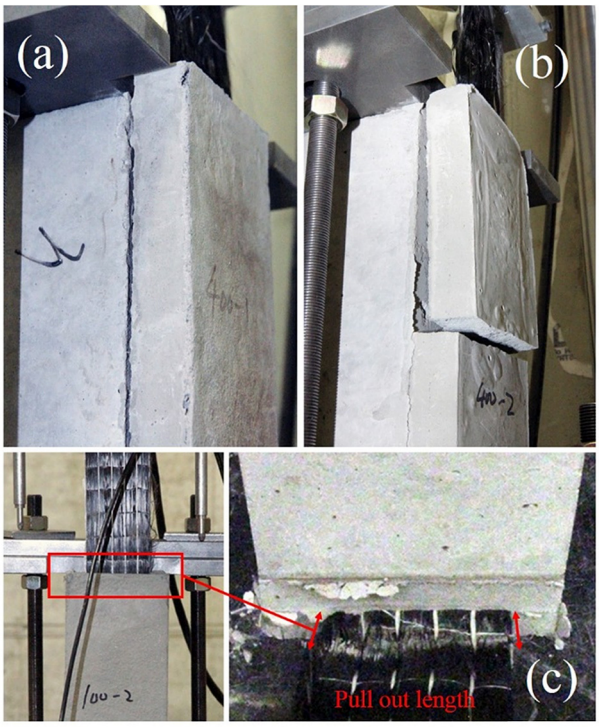

Fig. 12. Typical failure modes of the pull-out specimens: (a) interface debonding of ECC specimen; (b) interface debonding and mortar tensile cracking of mortar specimen, and (c) CFRP sheet being pulled out from the ECC layer.

Similarly, two failure modes were also observed for the mortar specimens in the pull-out tests. The CFRP sheet was pulled out from the mortar layer when the temperature was not higher than 300 °C. At 400 °C and 500 °C, the interface of the mortar layer and the concrete firstly debonded, and then the mortar layer fractured in tension under the loading transferred from the CFRP sheet (see Fig. 12(b)). This failure mode also matches the interface inspection of the mortar specimens in Fig. 11(b), which showed premature interface crack at temperatures above 400 °C before the pull-out test. The failure mode of the CFRP sheet being pulled out from the hybrid layer was similar for both ECC and mortar specimens, and one example is given in Fig. 12(c). Similar pulled-out failure was also observed for textile reinforced cementitious mortar strengthening systems as in Ref. [61].

The curves of stress versus the relative slip between CFRP and matrix (either ECC or mortar) under various temperatures are presented in Fig. 13. The stress, σ, is equal to the applied load, P, divided by the section area of CFRP sheet. The relative slip, δ, can be calculated by the following equation:

$$\delta = \Delta - \frac{PD}{WtE} \quad (1)$$

where Δ is the LVDT readings; D is the gauge length of LVDT (see Fig. 2); W and t are the width and thickness of CFRP sheet which are 50 mm and 0.55 mm respectively; E is the modulus of CFRP which was measured as 79.7 GPa.

In Fig. 13, the curves of the ECC specimens are denoted using solid symbols while the curves of the mortar specimens are plotted with hollow symbols. For ECC specimens under temperatures above 200 °C, the strengthening layer separated from the concrete during the pull-out tests (see Fig. 12(a)). Therefore, the curves of those specimens with the interface failure were not presented in Fig. 13(a). As can be seen in Fig. 13, the ECC and mortar specimens showed similar development of the pull-out stress against the relative slip between CFRP and matrix. Firstly, the stress increased with the slip up to a peak point after which a fast decrease of the stress was observed. Finally the stress became stabilized at a very low level (about 20 MPa) with the increase of the slip. The last stable stage of the stress was attributed to the friction between CFRP and the matrix (see Fig. 12(c)). It is obvious in Fig. 13(a) that the peak stress of ECC specimen seems not affected much by the temperature up to 200 °C. For the mortar specimens, the peak stress gradually decreased with the increase of temperature until a dramatic decrease in peak stress was observed at temperatures of 400 °C and 500 °C.

The peak stress of each specimen was extracted from the corresponding stress-slip curve and plotted against the temperature in Fig. 14(a) for ECC specimens and in Fig. 14(b) for mortar specimens. In Fig. 14, the symbol represents the average peak stress of repeating specimens and the error bar refers to the standard deviation. For ECC specimens in Fig. 14(a), the temperature effect on the peak pull-out stress is very similar to the temperature effect on the tensile properties of ECC in Fig. 10. The peak stress did not change much until 200 °C. The average peak stress at room temperature was 128.1 MPa. It decreased by only 1.7% to 125.9 MPa at 100 °C. At 200 °C, the peak stress was 119.9 MPa. When the temperature was higher than 200 °C, the peak stress dropped to zero. However, this does not mean that the CFRP-ECC hybrid could not sustain the pull-out force. This was because the specimens failed by the interface separation between the CFRP-ECC hybrid layer and the concrete due to the temperature treatment before the pull-out test. If the interface failure could have been avoided, the CFRP-ECC hybrid would highly likely to continue sustaining the pull-out loading (see the following detailed discussions).

Similarly, the peak stress of the mortar specimens in Fig. 14(b) also showed a two-stage behavior with the increase of the temperature. The average peak stress was 125.6 MPa at room temperature and 128.0 MPa at 100 °C. It decreased by 3.0%—121.8 MPa at 200 °C (comparing to the room temperature stress). A great drop in the peak stress was observed at 300 °C. It declined by 42.7%—72.0 MPa. When the temperature reached 400 °C and 500 °C, premature failure occurred at the interface between the CFRP-mortar hybrid layer and the concrete, followed by the mortar tensile cracking (see Fig. 12(b)). Due to this premature failure mode, the peak stress dropped dramatically to 11.2 MPa at 400 °C and 11.7 MPa at 500 °C.

Comparing the ECC and mortar specimens, the underlying mechanism that led to the reduction in the peak stress after 200 °C was totally different. For mortar specimens, the decrease of the peak stress after 200 °C was related to the material degradation of the mortar as discussed in Fig. 8. On the other hand, the ECC specimens failed at the interface between the CFRP-ECC hybrid layer and the concrete in the furnace when the temperature was higher than 300 °C. If the premature failure at the interface can be avoided, the CFRP-ECC hybrid may highly likely be able to sustain the pull-out force even with the temperature higher than 300 °C. In the current study, the surface treatment was used for bonding the hybrid layer to the concrete. It is recommended that shear keys be designed and installed on the concrete block before attaching the hybrid layer, so that the interface bonding between the hybrid and concrete can be secured.

4. Conclusions

In the current study, a CFRP-ECC hybrid was proposed for strengthening of concrete structures. The thermal-mechanical behavior of this hybrid was investigated through material testing and pull-out testing under elevated temperatures up to 500 °C. A

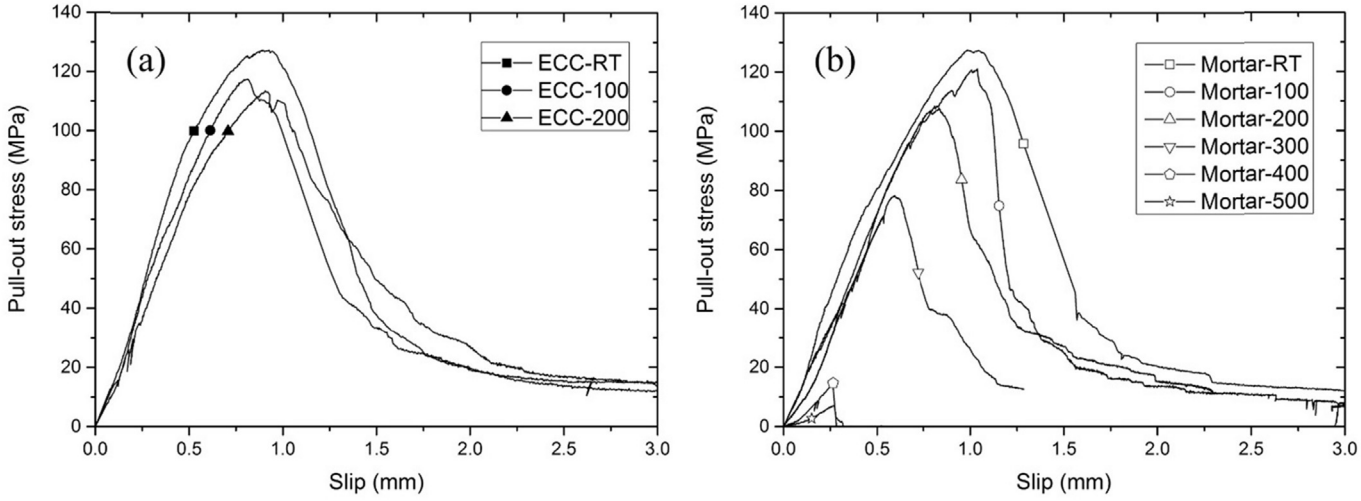

Fig. 13. Temperature effect on the pull-out stress-slip curves of the (a) ECC specimens and (b) mortar specimens.

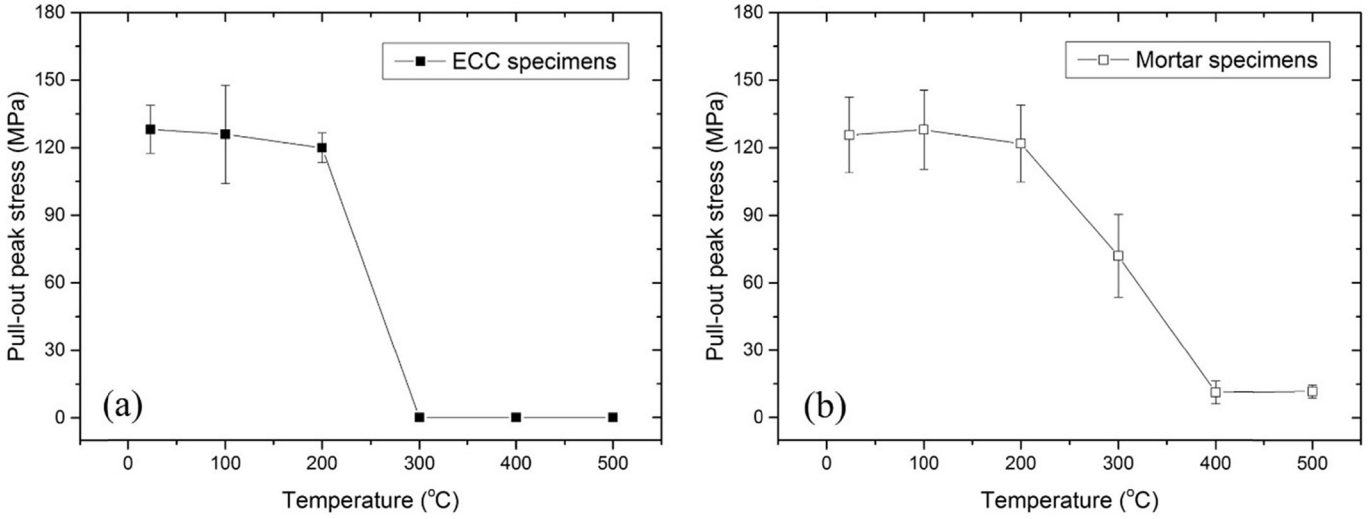

Fig. 14. Temperature effect on the peak pull-out stress of the (a) ECC specimens and (b) mortar specimens.

CFRP-mortar hybrid was also tested for comparison purpose. In the material testing, the effect of the elevated temperatures on the material properties (i.e. compressive strength, tensile strength and tensile strain capacity) of ECC and mortar were studied. In the pull-out testing, the pull-out stress versus the slip curves of the ECC and mortar specimens were derived. The temperature effect on the peak pull-out stress for both ECC and mortar specimens were compared. Based on the results in this paper, the following conclusions can be drawn:

(a) ECC cubes showed desirable anti-spalling behavior with the temperature up to 500 °C. The reason is that the PVA fibers melted creating interconnected channels. These channels helped the water vapor escape and the internal pressure of ECC was thus relieved. This anti-spalling mechanism of ECC was evidenced by the SEM investigations. Spalling of mortar cubes at 400 °C and 500 °C were observed.

(b) ECC has a better temperature performance in compression than that of mortar. For both ECC and mortar, the strength development with the temperature can be divided into two stages with a turning point at 300 °C. For ECC cubes, the compressive strength decreased by 4.8% in the first stage and by 31.3% in the second stage. For mortar cubes, the strength reduction in the first stage was 13.8%. At 400 °C and 500 °C, the mortar cubes spalled and no compression strength was measured.

(c) A similar two-stage tensile behavior under elevated temperatures was also observed for ECC. The turning point temperature was 200 °C. In the first stage, the strain hardening and multi cracking behavior of ECC was maintained. The tensile strength kept almost constant at around 4.9–5.2 MPa with a strain capacity of 1.3–1.7%. In the second stage, ECC failed in a brittle manner due to the melting of PVA fibers. The tensile strength dropped by 69.4% at 500 °C comparing to the strength at room temperature.

(d) Two competing mechanisms contributed to the two-stage compressive and tensile properties of ECC under elevated temperatures. The first was the pressure relieving mechanism through the interconnected channels created by the melted PVA fibers. The second mechanism was the

accumulated internal defects also related to the interconnected channels. In the first stage of the tension and compression behaviors, the first mechanism was dominant while the second mechanism became important in the second stage.

(e) It was found that a moderate temperature treatment up to 100 °C may effectively enhance the tensile properties of ECC.

(f) The interface between the CFRP-ECC hybrid and the concrete was more sensitive to the temperature treatment than that of the CFRP-mortar hybrid. For both ECC and mortar specimens, the CFRP sheet was pulled out from the hybrid layer when the temperature was no higher than 300 °C. At the temperatures above 400 °C, the CFRP-ECC hybrid debonded from the concrete under the pull-out loading, whereas the CFRP-mortar hybrid firstly debonded from the concrete and finally failed by mortar tensile cracking.

(g) A two-stage development of the peak pull-out stress with the temperature was observed for both ECC and mortar specimens. The turning point was 200 °C. For ECC specimens, the peak stress showed little change at around 120–130 MPa. The peak stress dropped to zero in the second stage due to the interface debonding. For mortar specimens, the peak stress was similar to that of ECC specimens in the first stage. In the second stage, the peak stress dropped to around 11 MPa.

It was recommended that shear keys be designed and installed on the concrete surface before attaching the CFRP-ECC hybrid layer. This is helpful to avoid the interface debonding between the hybrid layer and the concrete. In this way, the CFRP-ECC hybrid would have shown improved pull-out behavior under elevated temperatures.

Acknowledgments

The authors gratefully acknowledge the financial support provided by the Australian Ministry of Education through the Endeavour Research Fellowship scheme (BR14-003378/44882015) and the Thousand Talents Plan (Young Professionals) in China through the Fundamental Research Funds for the Central Universities (YWF-16-RSC-013). Mr. Danny Saltan helped with ordering the materials. Dr. Sukmin Kwon and Mr. Motohiro Ohno are acknowledged for their assistance with the experimental tests.

References

[1] Hollaway LC. Advanced polymer composites and polymers in the civil infrastructure. Oxford, UK: Elsevier; 2001.
[2] Bakis CE, Bank LC, Brown VL, Cosenza E, Davalos JF, Lesko JJ, et al. Fiber-reinforced polymer composites for construction-state-of-the-art review. J Compos Constr 2002;6(2):73–87.
[3] Hollaway LC, Teng JG. Strengthening and rehabilitation of civil infrastructures using fiber-reinforces polymers (FRP) composites. Cambridge, UK: Woodhead Publishing; 2008.
[4] Teng JG, Chen JF, Smith ST, Lam L. FRP strengthened RC structures. West Sussex, UK: John Wiley and Sons Ltd; 2002.
[5] Hollaway LC, Leeming MB. Strengthening of reinforced concrete structures: using externally-bonded FRP composites in structural and civil engineering. Cambridge, UK: Woodhead Publishing; 1999.
[6] Bank LC. Composites for construction : structural design with FRP materials. Hoboken, NJ: John Wiley & Sons; 2006.
[7] AC125. Acceptance criteria for concrete and reinforced and unreinforced masonry strengthening using fiber-reinforced polymer (FRP) composite systems. Whittier, CA: ICC Evaluation Service; 1997.
[8] ACI 440.2R-02. Guide for the design and construction of externally bonded FRP systems for strengthening concrete structures. Farmington Hills, MI: American Concrete Institute; 2002.
[9] FBI. Externally bonded FRP reinforcement for RC structures. Lausanne, Switzerland: International Federation for Structural Concrete; 2001.
[10] 55 TR. Design guidance for stengthening concrete structures using fibre composite materials. Surrey, England: The Concrete Society, Camberley; 2004.
[11] Hamilton HR, Benmokrane B, Dolan CW, Sprinkel MM. Polymer materials to enhance performance of concrete in civil infrastructure. Polym Rev 2009;49(1):1–24.
[12] Halliwell S. FRPs-the environmental agenda. Adv Struct Eng 2010;13(5):783–91.
[13] Nanni A. Concrete repair with externally bonded FRP reinforcement. Concr Int 1995;17(8):22–6.
[14] Yazdanbakhsh A, Bank LC. The effect of shear strength on load capacity of FRP strengthened beams with recycled concrete aggregate. Constr Build Mater 2016;102(1):133–40.
[15] Kalfat R, Al-Mahaidi R. Development of a hybrid anchor to improve the bond performance of multiple plies of FRP laminates bonded to concrete. Constr Build Mater 2015;94:280–9.
[16] Al-Tersawy SH. Effect of fiber parameters and concrete strength on shear behavior of strengthened RC beams. Constr Build Mater 2013;44:15–24.
[17] Czaderski C, Motavalli M. 40-Year-old full-scale concrete bridge girder strengthened with prestressed CFRP plates anchored using gradient method. Compos Part B Eng 2007;38(7–8):878–86.
[18] Ceroni F, Pecce M, Matthys S, Taerwe L. Debonding strength and anchorage devices for reinforced concrete elements strengthened with FRP sheets. Compos Part B Eng 2008;39(3):429–41.
[19] Aprile A, Feo L. Concrete cover rip-off of R/C beams strengthened with FRP composites. Compos Part B Eng 2007;38(5–6):759–71.
[20] El-Sayed AK. Effect of longitudinal CFRP strengthening on the shear resistance of reinforced concrete beams. Compos Part B Eng 2014;58:422–9.
[21] Michels J, Widmann R, Czaderski C, Allahvirdizadeh R, Motavalli M. Glass transition evaluation of commercially available epoxy resins used for civil engineering applications. Compos Part B Eng 2015;77:484–93.
[22] Dong K, Hu K. Development of bond strength model for CFRP-to-concrete joints at high temperatures. Compos Part B Eng 2016;95:264–71.
[23] Bai Y, Keller T. Effects of thermal loading history on structural adhesive modulus across glass transition. Constr Build Mater 2011;25(4):2162–8.
[24] Moussa O, Vassilopoulos AP, Keller T. Experimental DSC-based method to determine glass transition temperature during curing of structural adhesives. Constr Build Mater 2012;28(1):263–8.
[25] Petkova D, Donchev T, Wen J. Experimental study of the performance of CFRP strengthened small scale beams after heating to high temperatures. Constr Build Mater 2014;68:55–61.
[26] Ahmed A, Kodur VKR. Effect of bond degradation on fire resistance of FRP-strengthened reinforced concrete beams. Compos Part B Eng 2011;42(2):226–37.
[27] Firmo JP, Correia JR, Bisby LA. Fire behaviour of FRP-strengthened reinforced concrete structural elements: a state-of-the-art review. Compos Part B Eng 2015;80:198–216.
[28] López C, Firmo JP, Correia JR, Tiago C. Fire protection systems for reinforced concrete slabs strengthened with CFRP laminates. Constr Build Mater 2013;47:324–33.
[29] Tetta ZC, Koutas LN, Bournas DA. Shear strengthening of full-scale RC T-beams using textile-reinforced mortar and textile-based anchors. Compos Part B Eng 2016;95:225–39.
[30] Tetta ZC, Koutas LN, Bournas DA. Textile-reinforced mortar (TRM) versus fiber-reinforced polymers (FRP) in shear strengthening of concrete beams. Compos Part B Eng 2015;77:338–48.
[31] Hashemi S, Al-Mahaidi R. Experimental and finite element analysis of flexural behavior of FRP-strengthened RC beams using cement-based adhesives. Constr Build Mater 2012;26(1):268–73.
[32] Hashemi S, Al-Mahaidi R. Flexural performance of CFRP textile-retrofitted RC beams using cement-based adhesives at high temperature. Constr Build Mater 2012;28(1):791–7.
[33] D'Ambrisi A, Focacci F. Flexural strengthening of RC beams with cement-based composites. J Compos Constr 2011;15(5):707–20.
[34] Si Larbi A, Agbossou A, Hamelin P. Experimental and numerical investigations about textile-reinforced concrete and hybrid solutions for repairing and/or strengthening reinforced concrete beams. Compos Struct 2013;99:152–62.
[35] Elsanadedy HM, Almusallam TH, Alsayed SH, Al-Salloum YA. Flexural strengthening of RC beams using textile reinforced mortar-Experimental and numerical study. Compos Struct 2013;97:40–55.
[36] Triantafillou TC, Papanicolaou CG. Shear strengthening of reinforced concrete members with textile reinforced mortar (TRM) jackets. Mater Struct 2006;39(285):93–103.
[37] Tzoura E, Triantafillou TC. Shear strengthening of reinforced concrete T-beams under cyclic loading with TRM or FRP jackets. Mater Struct 2016;49(1):17–28.
[38] Li VC. On engineered cementitious composites (ECC). J Adv Concr Technol 2003;1(3):215–30.
[39] Li VC. Tailoring ECC for special attributes: a review. Int J Concr Struct Mater 2012;6(3):135–44.
[40] Tosun-Felekoğlu K, Felekoğlu B, Ranade R, Lee BY, Li VC. The role of flaw size and fiber distribution on tensile ductility of PVA-ECC. Compos Part B Eng 2014;56:536–45.
[41] Şahmaran M, Li VC. Durability of mechanically loaded engineered cementitious composites under highly alkaline environments. Cem Concr Compos 2008;30(2):72–81.
[42] Şahmaran M, Li VC. De-icing salt scaling resistance of mechanically loaded engineered cementitious composites. Cem Concr Res 2007;37(7):1035–46.
[43] Zhang J, Wang ZB, Ju XC. Application of ductile fiber reinforced cementitious composite in jointless concrete pavements. Compos Part B Eng 2013;50:

224–31.
[44] Sahmaran M, Lachemi M, Li VC. Assessing mechanical properties and microstructure of fire-damaged engineered cementitious composites. Mater J 2010;107(3):297–304.
[45] Yu JT, Lin JH, Zhang ZG, Li VC. Mechanical performance of ECC with high-volume fly ash after sub-elevated temperatures. Constr Build Mater 2015;99:82–9.
[46] Lepech MD, Li VC. Large-scale processing of engineered cementitious composites. ACI Mater J 2008;105(4):358–66.
[47] Lim YM, Li VC. Durable repair of aged infrastructures using trapping mechanism of engineered cementitious composites. Cem Concr Compos 1997;19(4):373–85.
[48] Li VC, Horii H, Kabele P, Kanda T, Lim YM. Repair and retrofit with engineered cementitious composites. Eng Fract Mech 2000;65(2–3):317–34.
[49] Maalej M, Leong KS. Engineered cementitious composites for effective FRP-strengthening of RC beams. Compos Sci Technol 2005;65(7–8):1120–8.
[50] Kim SW, Yun HD. Crack-damage mitigation and flexural behavior of flexure-dominant reinforced concrete beams repaired with strain-hardening cement-based composite. Compos Part B Eng 2011;42(4):645–56.
[51] Zheng YZ, Wang WW, Brigham JC. Flexural behaviour of reinforced concrete beams strengthened with a composite reinforcement layer: BFRP grid and ECC. Constr Build Mater 2016;115:424–37.
[52] Dai JG, Wang B, Xu SL. Textile reinforced engineered cementitious composites (TR-ECC) overlays for the strengthening of RC beams. Proceedings of the second Asia-Pacific Conferenceon Fiber Reinforced Polymers in Structures. Seoul, Korea, 2009.
[53] Huang X, et al. Development of green engineered cementitious composites using iron ore tailings as aggregates. Constr Build Mater 2013;44:757–64.
[54] C190/C190M-16a ASTM. Standard test method for compressive strength of hydraulic cement mortars (using 2-in. or [50-mm] cube specimens). West Conshohocken, PA: ASTM International; 2016.
[55] Felekoglu B, Tosun-Felekoglu K, Ranade R, Zhang Q, Li VC. Influence of matrix flowability, fiber mixing procedure, and curing conditions on the mechanical performance of HTPP-ECC. Compos Part B Eng 2014;60:359–70.
[56] JSCE. Recommendations for design and construction of high performance fiberreinforced cement composites with multiple fine cracks. Tokyo: Japan Society of Civil Engineers; 2008.
[57] ASTM D3039-14. Standard test method for tensile properties of polymer matrix composite materials. West Conshohocken, PA: ASTM International; 2014.
[58] ASTM C873/C873M. Standard test method for compressive strength of concrete cylinders cast in place in cylindrical molds. West Conshohocken, PA: ASTM International; 2015.
[59] Kalifa P, Menneteau FD, Quenard D. Spalling and pore pressure in HPC at high temperatures. Cem Concr Res 2000;30(12):1915–27.
[60] Luo X, Sun W, Chan SYN. Effect of heating and cooling regimes on residual strength and microstructure of normal strength and high-performance concrete. Cem Concr Res 2000;30(3):379–83.
[61] Ombres L. Analysis of the bond between fabric reinforced cementitious mortar (FRCM) strengthening systems and concrete. Compos Part B Eng 2015;69:418–26.